Journal of Geophysical Research: Solid Earth

Supporting Information for

Rayleigh Wave Attenuation and Amplification Measured at Ocean-Bottom Seismometer Arrays using Helmholtz Tomography

Joshua B. Russell[1], Colleen A. Dalton[1]

[1]Department of Earth, Environmental, and Planetary Sciences, Brown University, Providence, RI, USA

Contents of this file

Text S1.

1. Analytical expression for focusing correction due to geometrical spreading, $\nabla^2\tau_{GS}$

Here we derive an expression for the focusing/defocusing correction term (or wavefront curvature) due to geometrical spreading of a surface wave on a sphere. For simplicity, we consider the great-circle angular distance from an earthquake at the origin (0,0) to a point on Earth's surface at latitude, λ, and longitude, φ:

$$X = \cos^{-1}(\cos\lambda\cos\varphi) \tag{S1}$$

The travel time of a Rayleigh wave propagating with average phase velocity c from the origin to the point (λ, φ) is then expressed simply as

$$\tau = \frac{RX}{c} \tag{S2}$$

where R = 6371 km is the radius of the Earth. The Laplacian operator in spherical coordinates is applied to equation (S2), realizing that the term containing $\partial/\partial r$ goes to zero. After simplifying, we obtain the expression:

$$\nabla^2\tau = \frac{\cos\varphi\cos\lambda}{cR\sin X} \tag{S3}$$

Because we are considering geometrical spreading on a sphere, we can further simplify equation (S3) by assuming propagation along the equator (λ = 0):

$$\nabla^2 \tau \;=\; \frac{\cos X}{cR \sin X} \tag{S4}$$

Equation (S4) provides an expression for the wavefront curvature of a surface wave measured at an epicentral distance X from the earthquake source on a homogeneous sphere.

2. Analytical expression for apparent amplitude decay due to geometrical spreading

Similarly, we can derive an analogous expression for the apparent amplitude decay term (see equation (2) in the main text). The amplitude variation due to geometrical spreading of a surface wave across a sphere (ignoring attenuation) is expressed as

$$A = \frac{A_0}{\sqrt{2\pi R \sin X}} \tag{S5}$$

where A_0 represents Rayleigh-wave source excitation. By applying the gradient operator in spherical coordinates to equations (S2) and (S5) and taking their dot products, it can be shown that the normalized amplitude decay in the direction of propagation due to geometrical spreading is given by

$$\nabla \tau \cdot \frac{\nabla A}{A} \;=\; -\frac{\cos X}{2cR \sin X} \tag{S6}$$

Combining equations (S4) and (S6), we arrive at the transport equation for a non-attenuating medium:

$$2\nabla \tau \cdot \frac{\nabla A}{A} + \nabla^2 \tau = 0 \tag{S7}$$

3. Error propagation equations

Here we present the equations for propagating errors from the ray tomography estimates of the travel-time and amplitude gradient fields through each step to the apparent attenuation. The ray-tomography inversions from Section 3.3 provide formal estimates of uncertainty for travel-time gradient $\sigma_{\partial_x \tau}$ and $\sigma_{\partial_y \tau}$ as well as for normalized amplitude gradient $\sigma_{\partial_x A/A}$ and $\sigma_{\partial_y A/A}$. The augmented data kernel is given by (Menke, 2012)

$$\boldsymbol{F} = \begin{bmatrix} \boldsymbol{C}_d^{-1/2} \boldsymbol{G} \\ \frac{\varepsilon \lambda}{\Delta} \boldsymbol{H} \end{bmatrix} \tag{S8}$$

where $\boldsymbol{G}$ is the kernel containing geometry of the ray paths, $\boldsymbol{C}_d$ is the data covariance matrix containing the variance of each travel-time (or differential log amplitude) measurement along the diagonal, $\boldsymbol{H}$ is the second-derivative smoothing kernel, and $\varepsilon\lambda/\Delta$ is the smoothing weight as described in Section 3.3. The model covariance matrix is then given by

$$\boldsymbol{C}_m = [\boldsymbol{F}^T \boldsymbol{F}]^{-1} \tag{S9}$$

where diagonal elements provide the formal variance estimates of each model parameter σ_m^2 (i.e., $\sigma_{\partial_x \tau}^2$, $\sigma_{\partial_y \tau}^2$ in the case of the travel-time inversion and $\sigma_{\partial_x A/A}^2$, $\sigma_{\partial_y A/A}^2$ for the differential log amplitude inversion). This model covariance matrix accounts for both uncertainties in the data as well as the smoothing constraints applied.

Given measured uncertainties, σ_{x_i}, in model parameters $\boldsymbol{x} = [x_1, x_2, \dots, x_n]$, the corresponding error in a desired quantity $J(\boldsymbol{x})$ can be expressed analytically through the partial derivatives:

$$\sigma_J \approx \sqrt{\sum_{i=1}^{n} \left(\frac{\partial J(\boldsymbol{x})}{\partial x_i} \cdot \sigma_{x_i} \right)^2} \tag{S10}$$

Using this equation, we can propagate the uncertainties from $\boldsymbol{C}_m$ through all estimated components of the right-hand side of equation (6) in the main text as follows:

Travel-time gradient, $|\nabla \tau|$:

$$\sigma_{|\nabla \tau|} = \frac{\sqrt{(\partial_x \tau \cdot \sigma_{\partial_x \tau})^2 + \left(\partial_y \tau \cdot \sigma_{\partial_y \tau} \right)^2}}{|\nabla \tau|} \tag{S11}$$

Apparent phase velocity, c' :

$$\sigma_{c'} = \frac{1}{|\nabla \tau|^2} \sigma_{|\nabla \tau|} \tag{S12}$$

Focusing/defocusing correction term, $\nabla^2 \tau$:

$$\sigma_{\nabla^2 \tau} = \sqrt{\left(\frac{\partial^2 (\partial_x \tau)}{\partial x^2} \cdot \sigma_{\partial_x \tau} \right)^2 + \left(\frac{\partial^2 \left(\partial_y \tau \right)}{\partial y^2} \cdot \sigma_{\partial_y \tau} \right)^2} \tag{S13}$$

Amplitude decay term, $\frac{2\nabla A \cdot \nabla \tau}{A}$:

$$\sigma_{\left(\frac{2\nabla A \cdot \nabla \tau}{A} \right)} = \sqrt{\left(\partial_x \tau \cdot \sigma_{\partial_x A/A} \right)^2 + \left(\frac{\partial_x A}{A} \cdot \sigma_{\partial_x \tau} \right)^2 + \left(\partial_y \tau \cdot \sigma_{\partial_y A/A} \right)^2 + \left(\frac{\partial_y A}{A} \cdot \sigma_{\partial_y \tau} \right)^2} \tag{S14}$$

Final corrected amplitude decay (right-hand side of equation (6) in main text) $\frac{c}{2}\left(\frac{2\nabla A \cdot \nabla \tau}{A} + \nabla^2 \tau \right)$:

$$\sigma_{\frac{c}{2}\left(\frac{2\nabla A\cdot\nabla\tau}{A}+\nabla^2\tau\right)} = \sqrt{\left(\frac{1}{2}\left(\frac{2\nabla A\cdot\nabla\tau}{A}+\nabla^2\tau\right)\cdot\sigma_{c'}\right)^2+\left(\frac{c'}{2}\cdot\sigma_{\left(\frac{2\nabla A\cdot\nabla\tau}{A}\right)}\right)^2+\left(\frac{c'}{2}\cdot\sigma_{\nabla^2\tau}\right)^2} \quad \text{(S15)}$$

Supporting figures

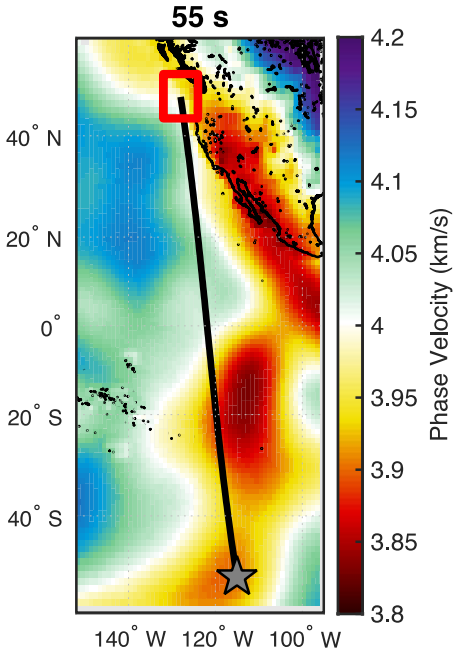

Figure S1. Source receiver geometry for the Mw 6.4 (May 12, 2014 13:58:21.5 GMT) shown in Figure 4. Phase velocities are from S362ANI+CRUST2.0. Red box shows the JdF study region.

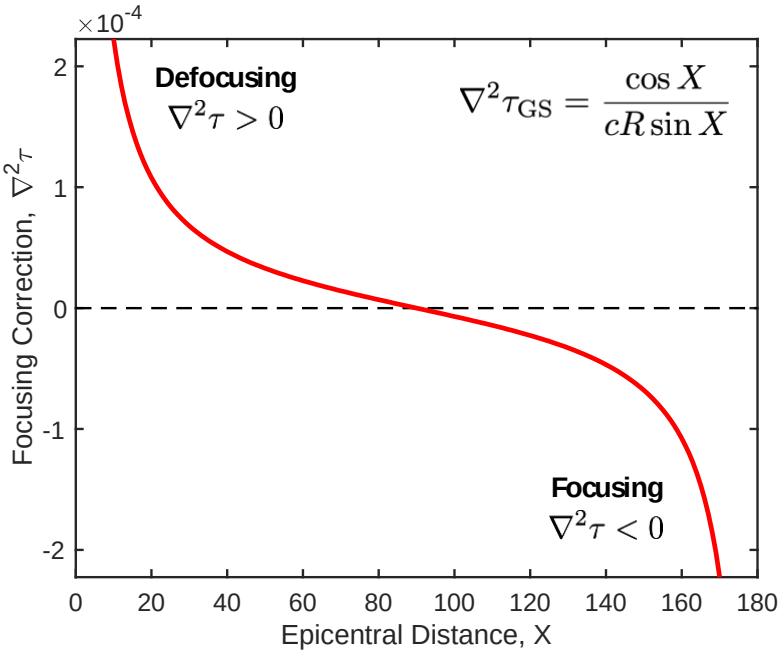

Figure S2. Focusing correction due to geometrical spreading for c = 4 km/s and R = 6371 km. Defocusing of the wavefield occurs at distances < 90º and focusing occurs at distances > 90º.

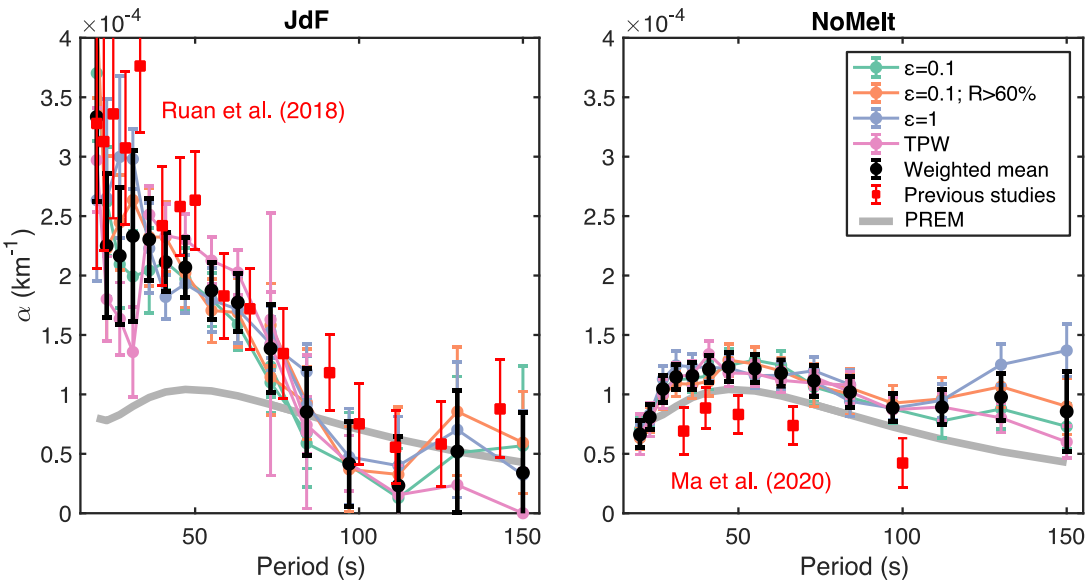

Figure S3. Attenuation measurements at (left) JdF and (right) NoMelt for different choices of smoothing parameter ε (purple; Equation 10) and quality control of event excitation (orange), in which only events with Rayleigh-wave excitation >60% of the maximum are considered. TPW measurements made on the same amplitude and phase dataset are shown in pink. The good agreement shows that our attenuation measurements are relatively insensitive to these choices. The black symbols denote the weighted mean and representative error bars that capture the range of uncertainties. Shown in red are previous studies that applied the TPW method to independently measured phase and amplitude datasets made using a Fourier Transform technique (Yang & Forsyth, 2006).

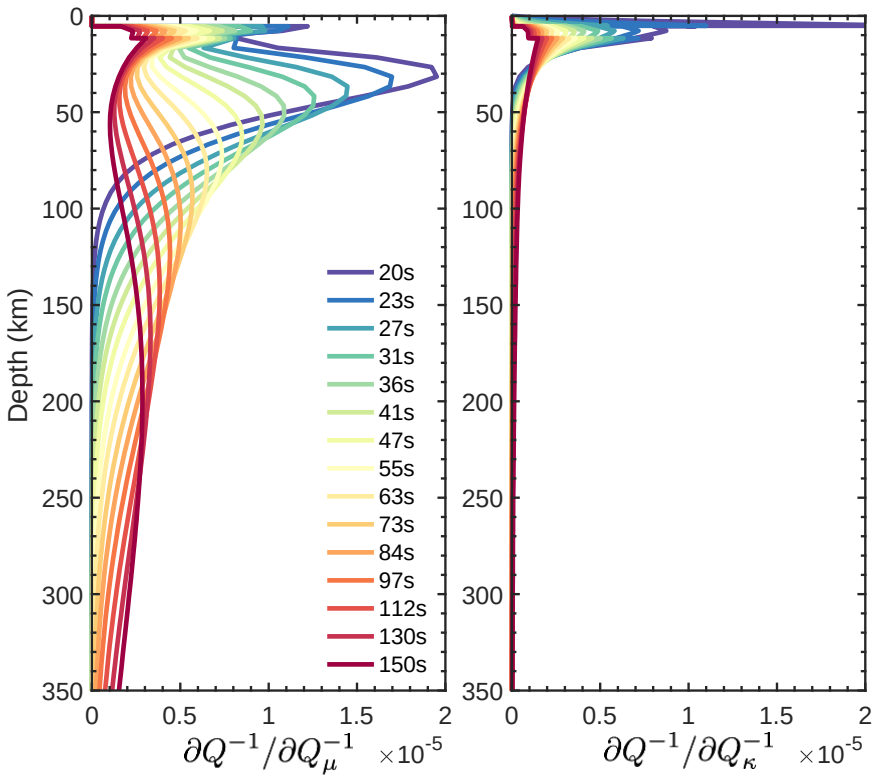

Figure S4. Example sensitivity kernels used in the 1-D inversions. (left) Sensitivity of Rayleigh wave attenuation to changes in shear attenuation Q_{μ}^{-1} and (right) bulk attenuation Q_{κ}^{-1}.

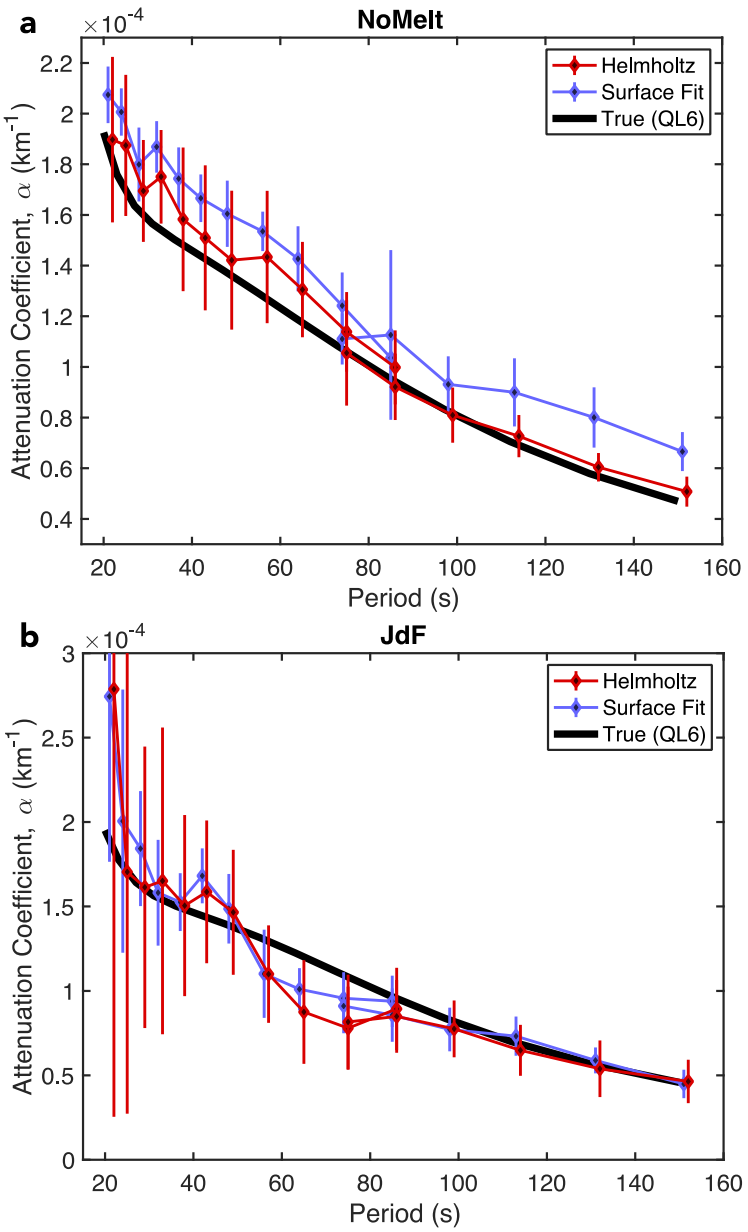

Figure S5. Recovery of synthetic 1-D attenuation using the Helmholtz tomography inversion presented in this paper (red; same as Figure 9 in the main text) compared to the surface fitting procedure of Lin et al. (2012) (purple). Results are shown for periods of 20–150 s at (a) NoMelt and (b) JdF. The input attenuation values of QL6 (Durek & Ekström, 1996) are shown in black. Attenuation is significantly overestimated at NoMelt at almost all periods using the surface fitting procedure. Overestimates of attenuation suggest a bias towards negative values of the focusing correction term (i.e. more *focusing* than expected) and/or the apparent amplitude decay term (i.e. measured amplitudes decay more rapidly than expected). Attenuation measured at JdF is comparable for the two techniques, but error bars are larger (and more realistic) for the Helmholtz inversion as uncertainties are propagated through each step.